1   **Mechanism of a COVID-19 nanoparticle vaccine candidate that elicits a broadly**

2   **neutralizing antibody response to SARS-CoV-2 variants**

3

4   Yi-Nan Zhang[1], Jennifer Paynter[1], Tatiana Fourfouris[1], Cindy Sou[1], Timothy Ngo[1], Linling He[1],

5   and Jiang Zhu[1, 2, *]

6

7   [1]Department of Integrative Structural and Computational Biology, [2]Department of Immunology

8   and Microbiology, The Scripps Research Institute, La Jolla, California 92037, USA

9

10

11   *Corresponding author

12   JZ: Phone +1 (858) 784-8157; Email: jiang@scripps.edu

13

14   **KEYWORDS**

15   Coronavirus disease 2019 (COVID-19); severe acute respiratory syndrome coronavirus 2

16   (SARS-CoV-2); variant of concern (VOC); vaccine; lymph node; germinal center; broadly

17   neutralizing antibody (bNAb).

18

ABSTRACT (150 words)

Vaccines against severe acute respiratory syndrome coronavirus 2 (SARS-CoV-2) are essential for combating the coronavirus disease 2019 (COVID-19) pandemic. Neutralizing antibody responses to the original Wuhan-Hu-1 strain that were generated during infection and vaccination showed lower effectiveness against variants of concern. Here, we demonstrated that mouse plasma induced by protein nanoparticles that present rationally designed S2GΔHR2 spikes can neutralize the B.1.1.7, B.1.351, and P.1 variants with comparable titers. The mechanism of nanoparticle vaccine-induced immunity was examined in mice for an I3-01v9 60-mer that presents 20 stabilized spikes. Compared with the soluble spike, this nanoparticle showed 6-fold longer retention, 4-fold greater presentation on follicular dendritic cell dendrites, and 5-fold higher germinal center reactions in lymph node follicles. Intact nanoparticles in lymph node tissues were visualized by transmission electron microscopy. In conclusion, spike-presenting protein nanoparticles that induce robust long-lived germinal centers may provide a vaccine solution for emerging SARS-CoV-2 variants.

ONE-SENTENCE SUMMARY (125 characters)

With prolonged lymph node retention and robust germinal centers, nanoparticles elicit neutralizing antibodies to diverse SARS-CoV-2 variants.

2

40   The COVID-19 pandemic has led to more than 124 million infection cases and 2.7 million deaths

41   globally. It has been reported that the human antibody responses to SARS-CoV-2 spike antigens

42   in COVID-19 patients can be sustained for several months after infection (*1-5*). However,

43   recently identified variants of concern (VOCs) exhibit higher transmissibility and resistance to

44   prior immunity as SARS-CoV-2 continues to adapt to the human host (*6, 7*). One such variant,

45   B.1.1.7, emerged from southeast England in October 2020 and accounted for two-thirds of new

46   infections in London in December 2020, with a higher transmission rate (43-90%) and risk of

47   mortality (32-104%) than previously circulating strains (*8-11*). Other variants, such as B.1.351

48   and P.1, also became prevalent in the Eastern Cape, Western Cape, and KwaZulu-Natal

49   provinces in South Africa and in Manaus, Brazil, respectively (*7, 12-14*). The rise of SARS-

50   CoV-2 VOCs and their rapid spread worldwide will likely result in more infection cases,

51   hospitalizations, and potentially more deaths, further straining healthcare resources (*14*).

52   To date, seven COVID-19 vaccines have been approved for emergency use in humans,

53   with more than 100 candidates being assessed in various phases of clinical trials (*15*). With the

54   exception of inactivated whole-virion vaccines, diverse platforms have been used to deliver the

55   recombinant SARS-CoV-2 spike, such as mRNA-encapsulating liposomes (e.g., BNT162b2 and

56   mRNA-1273), adenovirus vectors (e.g., ChAdOx1 nCoV-19 [AZD1222], CTII-nCoV, Sputnik

57   V, and Ad26.COV2.S), and nanoparticles (e.g., NVX-CoV2373). These vaccines demonstrated

58   65-96% efficacies in Phase 3 trials, with reduced morbidity and mortality associated with

59   COVID-19 disease (*16-20*). However, a notable loss of vaccine efficacy against new SARS-

60   CoV-2 variants was reported because of spike mutations in the receptor-binding domain (RBD;

61   e.g., K417N, E484K, and N501Y), N-terminal domain (NTD; e.g., L18F, D80A, D215G, and

62   Δ242-244), and other regions that are critical to spike stability (e.g., D614G) (*7, 21-28*). Among

63   circulating VOCs, the B.1.351 lineage appeared to be most resistant to neutralization by

64   convalescent plasma (9.4-fold) and vaccine sera (10.3- to 12.4-fold) (*29*), while a lesser degree

65   of reduction was observed for an early variant, B.1.1.7 (*30, 31*). Based on these findings, it was

66   suggested that vaccines would need to be updated periodically to maintain protection against

67   rapidly evolving SARS-CoV-2 (*24, 32, 33*). This raises the concern that herd immunity may not

68   be achievable with current vaccines and highlights the necessity of developing vaccines that can

69   elicit a broadly neutralizing antibody (bNAb) response to SARS-CoV-2 variants (*24, 28*). As

70   previously reported (*34-40*), the production of a bNAb response relies on long-lived germinal

71   center (GC) reactions to activate precursor B cells, stimulate affinity maturation, and form long-

72   term immune memory. Antigen retention and presentation within lymph node follicles are key to

73   the induction of long-lived GC reactions (*34, 36*) and thus should be a main criterion in the

74   development of bNAb-producing vaccines.

75   We previously investigated the cause of SARS-CoV-2 spike metastability and rationally

76   designed the S2GΔHR2 spike, which was displayed on three self-assembling protein

77   nanoparticle (SApNP) platforms, including ferritin (FR) 24-mer and multilayered E2p and I3-

78   01v9 60-mers, as COVID-19 vaccine candidates (*41*) (**Fig. 1A**). Notably, the I3-01v9 SApNP

79   that presents 20 stabilized spikes induced a potent NAb response against both SARS-CoV-1 and

80   SARS-CoV-2, in addition to critically needed T cell responses (*41*). Here, we first examined the

81   neutralizing activity of mouse plasma induced by these rationally designed vaccine constructs

82   against representative SARS-CoV-2 variants. We then investigated how SApNPs "behave" in

83   lymph nodes and induce GCs in the mouse model by characterizing vaccine delivery and

84   immunological responses at the intraorgan, intracellular, and intercellular levels. Our findings

4

85   suggest that a spike-presenting protein nanoparticle vaccine may confer broad protection against

86   SARS-CoV-2 VOCs.

87   We first assessed the neutralizing activity of polyclonal plasma elicited by various spike

88   and SApNP vaccine formulations in pseudoparticle (pp) neutralization assays (*42*). Mouse

89   plasma at week 5 after intraperitoneal (i.p.) injections of adjuvanted vaccine antigens (50 µg)

90   from our previous study were analyzed against the original SARS-CoV-2 strain, Wuhan-Hu-1, as

91   a baseline for comparison (**Fig. 1B**). The soluble $S2P_{ECTO}$ spike elicited the lowest 50%

92   inhibitory dilution (ID_{50}) titers, whereas the soluble S2GΔHR2 spike induced a stronger NAb

93   response, showing a 7.1-fold higher (or 8.1 times) average ID_{50} titer, which did not reach

94   statistical significance because of within-group variation. All three spike SApNP vaccines

95   elicited superior neutralizing antibody responses compared with the soluble $S2P_{ECTO}$ spike (*41,*

96   *43*). Notably, the I3-01v9 SApNP vaccine showed the most potent NAb response, with an

97   average ID_{50} titer of 2090, which was 8.1-fold higher than the soluble $S2P_{ECTO}$ spike. Despite the

98   differences in ID_{50} titers, the overall pattern remained the same as observed in our previous study

99   (*41*). These differences can be attributed to the inherent variation of pseudovirus neutralization

100   assays (*42*) (see Methods).Next, we assessed neutralizing activity against three major SARS-

101   CoV-2 variants (**Fig. 1C**, **fig. S1A, B**). The I3-01v9 SApNP induced a stronger NAb response

102   against three VOCs, with 0.5-fold (B.1.1.7), 0.8-fold (B.1.351), and 1.8-fold (P.1) higher ID_{50}

103   titers compared with the Wuhan-Hu-1 strain (**Fig. 1C**). These results were confirmed in a second

104   experiment, in which mice were intraperitoneally immunized with low doses (5 and 15 µg) of I3-

105   01v9 SApNP. Remarkably, all three SARS-CoV-2 VOC-pps were neutralized by mouse plasma,

106   with ID_{50} titers comparable to the high-dose group (45 µg; **fig. S1C, D**). To examine whether

107   routes of injection affect the elicitation of NAb responses against VOCs, we performed a third

108 experiment, in which a low dose (3.3 μg) of adjuvanted antigen was intradermally administered

109 into four footpads (i.e., 0.8 μg/footpad). The large (~55-60 nm) E2p and I3-01v9 SApNPs that

110 present 20 S2GΔHR2 spikes yielded higher ID_{50} titers than the soluble S2GΔHR2 spike (**Fig.**

111 **1D**, **fig. S1E, F**), whereas a significant reduction of neutralizing titers against the variants was

112 observed for mouse plasma from the S2GΔHR2 group (**Fig. 1E**, **fig. S1E, F**), suggesting that

113 nanoparticle display is critical for eliciting a bNAb response. The E2p and I3-01v9 SApNP

114 groups exhibited comparable or stronger NAb responses against three variants relative to the

115 original Wuhan-Hu-1 strain (**Fig. 1E**). A panel of human NAbs was previously used to validate

116 the SARS-CoV-2-pp neutralization assays, in addition to evaluating the antigenicity of rationally

117 designed spikes and SApNPs (*41*). This panel of human NAbs was tested against SARS-CoV-2-

118 pps that carry various VOC spikes (**Fig. 1F**, **fig. S1G**). Lower potency, measured by the 50%

119 inhibitory concentration (IC_{50}), was observed for all human NAbs against B.1.351 and P.1

120 variants, with the exception of NAb S309, which was identified from a SARS-CoV-1 patient

121 (*44*). This finding is consistent with previous reports on convalescent patient plasma (*29-31*). As

122 a negative control, mouse plasma induced by the S2GΔHR2-presenting I3-01v9 SApNP was

123 tested against pseudoviruses carrying the murine leukemia virus (MLV) Env, or MLV-pps.

124 Nonspecific neutralization was not detected (**fig. S1H, I**). Altogether, these results demonstrated

125 a clear advantage of spike-presenting SApNPs in eliciting a strong bNAb response against

126 SARS-CoV-2 VOCs compared with soluble spikes.

127   Next, we studied *in vivo* behaviors of the S2GΔHR2 spike and two large SApNPs to

128 understand vaccine-induced immunity and why nanoparticles outperform soluble spikes in terms

129 of bNAb elicitation. We first examined the distribution of S2GΔHR2-presenting I3-01v9

130 SApNPs in mouse lymph nodes via footpad injection (10 μg). The mice were sacrificed 12 h

131   after single-dose (**Fig. 2A**) and prime-boost (**Fig. 2B**) regimens. The axillary, brachial, and

132   popliteal sentinel lymph nodes were isolated for histological analysis. The lymph node tissues

133   were stained with the human anti-spike antibody P2B-2F6 (*45*) to characterize SARS-CoV-2

134   spikes presented on the I3-01v9 SApNPs. Consistent with our previous study (*46*), SApNPs

135   accumulated in lymph node follicles, regardless of the number of doses. SApNPs were

136   sequestered in the center of lymph node follicles after a single-dose (**Fig. 2A,** images on the left,

137   schematics on the right), but were located along the outer layer of expanded lymph node follicles

138   after the second injection due to preexisting humoral immunity (i.e., GC reactions) that was

139   induced by the first dose (**Fig. 2B**, images on the left, schematics on the right). Overall, the

140   majority of SApNPs accumulated in lymph node follicles, while their distribution differed

141   slightly depending on the doses.

142   In this context, we examined patterns of trafficking and lymph node follicle retention for

143   soluble S2GΔHR2 spike *vs.* the S2GΔHR2-presenting E2p and I3-01v9 SApNPs. To facilitate

144   this analysis, the mice were sacrificed 2 h to 8 weeks after a single dose (**Fig. 2C**) and 2 h to 5

145   weeks after the boost (**Fig. 2D**). The injection dose was normalized to the total amount of protein

146   (10 μg) per injection into each footpad (40 μg/mouse). As shown in **Fig. 2C**, the S2GΔHR2

147   spikes that trafficked into lymph node follicles at 2 h cleared within 48 h. In contrast, the two

148   large SApNPs accumulated in the subcapsular sinus at 2 h and then trafficked into follicles 12 h

149   after the single-dose injection. Remarkably, I3-01v9 SApNPs remained detectable in lymph node

150   follicles after 2 weeks, suggesting 6-fold longer retention than the S2GΔHR2 spike (**Fig. 2C**).

151   The results for these protein nanoparticles are thus consistent with the pattern of size dependency

152   that was observed for ovalbumin-conjugated gold nanoparticles in our previous study (*46*), in

153   which small (5-15 nm) nanoparticles cleared shortly after the injection, whereas large (50-100

154   nm) nanoparticles were retained in lymph node follicles for weeks. Similar patterns of antigen

155   retention were observed after the second injection, although the boost appeared to exert a more

156   positive effect on the soluble spike, which could be detected in lymph node follicles at 48 h (**Fig.**

157   **2D**). Nonetheless, prolonged retention was observed for both E2p and I3-01v9 SApNPs 2 weeks

158   after the boost injection. Overall, the multivalent display of S2GΔHR2 spikes on the I3-01v9

159   SApNP resulted in 325- and 4-fold greater accumulation in lymph node follicles compared with

160   the soluble spike 48 h after the single-dose **(Fig. 2E)** and prime-boost **(Fig. 2F)** injections,

161   respectively. These findings reveal the advantage of a leading vaccine candidate identified in our

162   previous study, S2GΔHR2-10GS-I3-01v9-L7P (*41*), in terms of spike antigen retention in lymph

163   node follicles.

164   Next, we determined the involvement of resident cells in antigen retention in lymph node

165   follicles. Recent studies reported that follicular dendritic cells (FDCs) are resident stromal cells

166   in follicles and can retain immune complexes, virus-like particles, virus, and bacteria (*46-51*).

167   Follicular dendritic cells are key to naive antigen retention, GC initiation and maintenance, and B

168   cell affinity maturation (*39, 52-55*). Here, we hypothesized that FDCs comprise the major cell

169   population in lymph node follicles that retain SARS-CoV-2 spikes and spike-presenting

170   SApNPs. To test this hypothesis, we administered vaccines via footpad injections and collected

171   mouse lymph nodes at the peak of accumulation (12 h) after single-dose (**Fig. 3A**) and prime-

172   boost (**Fig. 3B**) injections. Lymph node tissue samples were stained with the anti-spike antibody

173   P2B-2F6 (*45*) for the spike antigen and anti-CD21 and CD169 antibodies for FDCs and

174   subcapsular sinus macrophages, respectively. The S2GΔHR2 spike and SApNP (E2p or I3-01v9)

175   signals colocalized with FDC (CD21^{+}) networks in lymph node follicles (**Fig. 3A, B**). This result

8

176   confirmed the critical role of FDC networks in mediating vaccine retention in lymph node

177   follicles.

178   The induction of potent bNAb responses by spike-presenting SApNPs (**Fig. 1**) suggests

179   the effective activation of naïve B cells and subsequent recalls by crosslinking B cell receptors

180   (*56-58*). However, still unclear are the manners in which FDC networks present SApNPs to B

181   cells to trigger such a bNAb response. Here, we analyzed the interface between FDC networks

182   and B cells by transmission electron microscopy (TEM). Briefly, fresh lymph nodes were

183   isolated and directly immersed in fixative. The processed tissue samples were sectioned and

184   stained on copper grids for TEM analysis. We first determined whether SApNPs, such as the

185   S2GΔHR2-presenting I3-01v9 SApNP, remain intact *in vivo* (**fig. S2**). Mouse lymph nodes were

186   isolated 2 h after the injection of a high dose (50 μg) of the non-adjuvanted I3-01v9 SApNP. The

187   TEM images revealed that round-shape granules corresponding to intact SApNP aligned on the

188   macrophage surface or inside endolysosomes of the macrophage in a lymph node (**fig. S2**). We

189   next studied the relative location between FDCs and I3-01v9 SApNPs and how FDCs present

190   SApNPs to B cells. Mouse lymph nodes were collected 2, 12, and 48 h after a single-dose (50

191   μg) and 12 h after the boost of the I3-01v9 SApNP vaccine. The FDCs exhibited the

192   characteristic morphology of long dendrites that surrounded and interacted with B cells in lymph

193   node follicles (**Fig. 3C**, **fig. S3**). While few I3-01v9 SApNPs were observed on FDC dendrites at

194   2 h (**fig. S3D**), notably more nanoparticles migrated to and aligned on FDC dendrites at 12 and

195   48 h (**Fig. 3C**, **figs. S3A-C**, yellow arrows). The TEM images indicated that FDCs can present

196   many SApNPs to neighboring B cells in this "hugging mode", in which their long dendrites

197   brace B cells to maximize interactions between multivalently displayed spikes and B cell

198   receptors. These results demonstrated the intrinsic nature of FDCs as a reservoir for the

199   sequestration, retention, and presentation of virus-like particles, or SApNPs with similar

200   molecular traits, to initiate GC reactions.

201   Lastly, we investigated whether the prolonged retention of S2GΔHR2-presenting E2p and

202   I3-01v9 SApNPs induce more robust GCs in lymph node follicles than the soluble S2GΔHR2

203   spike. Immunohistological analysis was performed to characterize GC B cells (GL7$^+$) and T

204   follicular helper (T$_{fh}$) cells (CD4$^+$Bcl6$^+$). For the I3-01v9 SApNP, 2 weeks after immunization,

205   we observed robust GCs in lymph node B cell follicles (B220$^+$) with well-formed dark zone

206   (DZ) and light zone (LZ) compartments, which contain GC B cells, FDCs, and T$_{fh}$ cells (*35, 37,*

207   *59-62*) (**Fig. 4A**). We then extended the analysis to the S2GΔHR2 spike and spike-presenting

208   SApNPs 2, 5, and 8 weeks after the single-dose injection (**Fig. 4B, fig. S4A-C**) and 2 and 5

209   weeks after the boost (**Fig. 4C, fig. S4D, E**). Two semi-quantitative metrics, the GC/FDC ratio

210   (i.e., whether GC formation is associated with an FDC network, %) and GC size (i.e., occupied

211   area), were used in this analysis. Overall, the soluble S2GΔHR2 spike and both large SApNPs

212   induced robust GCs 2 weeks after immunization (**Fig. 4B, fig. S4A**). The E2p and I3-01v9

213   SApNPs that present 20 S2GΔHR2 spikes induced robust, long-lived GCs, whereas the spike

214   alone failed to sustain robust GCs at week 8 with either the single-dose (**Fig. 4B, D**) or prime-

215   boost (**Fig. 4C, E**) injections. The I3-01v9 SApNP generated larger GCs than the soluble spike,

216   2.0-fold larger after the single-dose (**Fig. 4B, D**) and 2.4-fold larger after the boost (**Fig. 4C, E**),

217   measured at week 8.

218   We further characterized GC reactions by flow cytometry. Fresh mouse lymph nodes

219   were disaggregated into a single cell suspension and stained with an antibody cocktail to quantify

220   GC B cells and T$_{fh}$ cells (**fig. S5A**). The results were consistent with the immunohistological

10

221   analysis, in which all spike-based vaccine antigens, including the S2GΔHR2 spike and SApNPs,

222   showed robust GCs at week 2 after the injection that declined over time, as measured at weeks 5

223   and 8 (**Fig. 4F**). The E2p and I3-01v9 SApNPs generated a larger population of GC B cells than

224   both the S2P$_{ECTO}$ and S2GΔHR2 spikes at week 2 (**fig. S5B, C**). Although the boost dose had

225   little impact on the frequency of GC B cells and T$_{fh}$ cells, it appeared to extend GC formation

226   within lymph nodes (**Fig. 4F, G**), which may promote B cell development toward bNAbs.

227   Notably, the GC B cell and T$_{fh}$ cell populations elicited by the soluble S2GΔHR2 spike were

228   barely detectable 5 weeks after immunization (**Figs. 4F, G**). This result was reminiscent of a

229   recent study of an mRNA vaccine, in which GC reactions diminished to baseline levels at week 4

230   after a single-dose injection (*63*). The S2GΔHR2-presenting I3-01v9 SApNP generated 3.7/5.2-

231   fold more GC B cells and 3.7/4.4-fold more T$_{fh}$ cells than the soluble S2GΔHR2 spike after

232   one/two-dose immunization at week 8 (**Fig. 4G**). Therefore, SApNPs that were retained on FDC

233   dendrites could present SARS-CoV-2 neutralizing epitopes to enable more effective B cell

234   recognition than the soluble spike, and consequently induce more robust and long-lived GCs in

235   lymph nodes.

236   To end the COVID-19 pandemic, vaccines need to effectively block current and

237   emerging SARS-Cov-2 variants that evade NAb responses by mutating key epitopes on the viral

238   spike (*24*). Such vaccines must induce long-lasting GCs to facilitate the development of bNAbs.

239   Effective vaccine retention and presentation are critical for inducing and sustaining GC

240   reactions, which in turn promote the proliferation and affinity maturation of antigen-specific B

241   cells. Here, we found that the S2GΔHR2-presenting I3-01v9 SApNP, a vaccine candidate from

242   our recent study (*41*), elicited 6-fold longer retention and 4-fold greater accumulation in lymph

243   node follicles than the stabilized S2GΔHR2 spike alone with a prime-boost regimen (**Fig. 2D, F**).

11

244   This can be attributed to the intrinsic physiological properties of lymph nodes that mediate

245   vaccine trafficking and retention in follicles in a size-dependent manner, which would favor

246   retaining large (> 50 nm) virus-like nanoparticles (*46-48, 64, 65*). Supporting this notion are the

247   images of retained I3-01v9 SApNPs aligned on long FDC dendrites, suggesting that such protein

248   nanoparticles can present spike antigens to B cells for rapid initiation and then sustain GC

249   reactions in lymph node follicles for an extended period of time (**Fig. 3, 4**). Specifically, the

250   S2GΔHR2-presenting I3-01v9 SApNP generated 2.4-fold larger GCs and greater numbers of GC

251   B cells (5.2-fold) and T_{fh} cells (4.4-fold) than the soluble S2GΔHR2 spike with the prime-boost

252   regimen (**Fig. 4**). The findings in this study provide quantitative evidence that spike-presenting

253   SApNP vaccines are uniquely suited for inducing long-lived robust GCs in lymph node follicles.

254   Our analyses also provide potential explanations for the mechanism by which the S2GΔHR2-

255   presenting I3-01v9 SApNP can elicit a more effective bNAb response than the soluble spike (**Fig.**

256   **1B**) (*32*). Further investigation at the monoclonal level will reveal how bNAbs recognize

257   conserved epitopes and facilitate the rational design of SARS-CoV-2 spike antigens (*24*).

258   Superior NAb responses have been reported for other COVID-19 vaccine candidates that take

259   advantage of particulate display (*66-78*). Importantly, our S2GΔHR2-presenting I3-01v9 SApNP

260   vaccine elicited bNAb responses to three SARS-CoV-2 VOCs (**Fig. 1**), thus meeting a major

261   criterion for next-generation COVID-19 vaccines.

262   Protein vaccines have well-established records of both safety and effectiveness (*79-82*),

263   but they have yet to be deployed in the global campaign against the COVID-19 pandemic.

264   Through formulation with adjuvants to further enhance immune responses (*83-88*), protein

265   vaccines can be used either alone or as a booster for currently used nucleic acid vaccines. One

266   such protein vaccine, NVX-CoV2373 (full-length S2P spikes formulated with Matrix-M^{TM}

12

267   adjuvant), showed 96.4% efficacy in human trials (*89*). In our studies, we formulated the spike-

268   presenting E2p and I3-01v9 SApNPs with the AddaVax and aluminum phosphate adjuvants (*41*),

269   which induced stronger GC reactions than non-adjuvanted SApNPs at week 2 (**fig. S6**). Further

270   development of these SApNP vaccines may benefit from a systematic analysis of adjuvants that

271   target diverse immune pathways. An in-depth understanding of how different vaccine platforms

272   (e.g., inactivated virions, mRNAs, viral vectors, and nanoparticles) behave *in vivo*, such as

273   trafficking and retention in lymph nodes, interactions with immune cells, antigen processing and

274   presentation, and GC reactions and NAb responses, will provide insights into vaccine-induced

275   immunity (*82, 90-92*). This knowledge will in turn accelerate vaccine development against

276   SARS-CoV-2 and other emerging pathogens.

277   **MATERIALS AND METHODS**

278   **SARS-CoV-2 spike and SApNP vaccine antigens**

279   The design, expression, and purification of a stabilized SARS-CoV-2 spike, S2GΔHR2, and

280   three SApNPs that present either 8 or 20 S2GΔHR2 spikes were described in our recent study

281   (*41*). Briefly, the spike gene of the SARS-CoV-2 isolate Wuhan-Hu-1 (GenBank accession no.

282   MN908947) was modified to include the mutations ^{682}GSAGSV^{687} and K986G/V987G, in

283   addition to truncation of the HR2 stalk (ΔE1150-Q1208). The viral capsid protein SHP (Protein

284   Data Bank: 1TD0) was added as a C-terminal trimerization motif to stabilize the S2GΔHR2

285   trimer, resulting in a soluble S2GΔHR2-5GS-1TD0 spike (*41*). The S2GΔHR2 spike was

286   genetically fused to FR, multilayered E2p, and multilayered I3-01v9 with 5GS, 5GS, and 10GS

287   linkers, respectively, resulting in three S2GΔHR2-presenting SApNPs (*41*). An S2P$_{ECTO}$-5GS-

288   1TD0 spike construct that contained the mutations ^{682}GSAGSV^{687} and K986G/V987G but

289   without HR2 deletion (*41*) was included for comparison. All of the vaccine antigens were

13

290   transiently expressed in ExpiCHO cells and purified by a CR3022 antibody column and size-

291   exclusion chromatography (SEC) on a Superose 6 10/300 GL column as described previously

292   (*41*).

293

294   **Animal immunization and sample collection**

295   Similar immunization protocols were reported in our previous vaccine studies (*41, 93-95*).

296   Briefly, Institutional Animal Care and Use Committee (IACUC) guidelines were followed for all

297   of the animal studies. BALB/c mice (6 weeks old) were purchased from The Jackson Laboratory

298   and kept in ventilated cages in environmentally controlled rooms at The Scripps Research

299   Institute. The mouse studies were conducted according to Association for the Assessment and

300   Accreditation of Laboratory Animal Care guidelines, and the protocols were approved by the

301   IACUC. For the immunogenicity study, the mice were intraperitoneally immunized at either

302   weeks 0 or 3 with 200 μl of antigen/adjuvant mix containing 5-50 μg of vaccine antigen and 100

303   μl of adjuvant (*41*) or immunized at weeks 0 and 3 with 20 μl of antigen/adjuvant mix containing

304   0.8 μg of vaccine antigen per injection (3.3 μg/mouse) and 10 μl of adjuvant per injection (four

305   footpads were injected with a total of 80 μl [20 μl/footpad]) via intradermal footpad injections.

306   For the mechanism study of vaccine trafficking, retention, and induced GCs, the mice were

307   immunized at weeks 0 and 3 with 20 μl of antigen/adjuvant mix containing 10 μg of vaccine

308   antigen and 10 μl of adjuvant per injection. To visualize S2GΔHR2-presenting I3-01v9 SApNPs

309   in lymph node tissues using TEM, the mice were immunized at weeks 0 and 3 with 70 μl of

310   antigen/adjuvant mix containing 50 μg of vaccine antigen and 20 μl of adjuvant per injection.

311   Vaccines were administered into intradermal footpads of mice using a 29-gauge insulin needle

312   under 3% isoflurane anesthesia with oxygen. Blood was drawn from the maxillary/facial vein

14

313   into an ethylenediaminetetraacetic acid (EDTA)-coated tube 2 weeks after each immunization.

314   Blood plasma was isolated after centrifugation at 14000 rotations per minute (rpm) for 10 min.

315   Plasma was heated and inactivated at 56°C for 30 min. The supernatant was then collected after

316   centrifugation at 8000 rpm for 10 min. Plasma was used for the neutralization assay to determine

317   neutralizing antibody responses. The axillary, brachial, and popliteal sentinel lymph nodes were

318   collected at the end timepoint for further analysis.

319

320   **SARS-CoV-2 pseudovirus neutralization assay**

321   The SARS-CoV-2-pp neutralization assays were described in our previous study (*41*). Briefly,

322   SARS-CoV-2-pps were generated by the co-transfection of HEK293T cells with the HIV-1

323   pNL4-3.lucR-E- plasmid (obtained from the National Institutes of Health AIDS reagent program;

324   https://www.aidsreagent.org/) and the expression plasmid encoding the S gene of various SARS-

325   CoV-2 strains, including three variants: B.1.1.7, B.1.351, and P.1 (GISAID accession no.

326   EPI_ISL_601443, EPI_ISL_678597, and EPI_ISL_792680, respectively). The HEK293T-

327   hACE2 cell line (catalog no. NR-52511) and pcDNA3.1(-) vector containing the S gene of the

328   SARS-CoV-2 isolate Wuhan-Hu-1 (catalog no. NR52420) were requested from the BEI

329   Resources (https://www.beiresources.org/) on September 23, 2020 and used in the pseudovirus

330   neutralization assays (*42*). Based on sequence alignment, spike mutations were incorporated into

331   the S gene of the original Wuhan-Hu-1 isolate (catalog no. NR52420) to create respective

332   expression plasmids for B.1.1.7, B.1.351, and P.1. SARS-CoV-2-pp neutralization by immunized

333   mouse plasma and human monoclonal antibodies (mAbs) was performed according to a

334   previously described protocol (*41*). Using the same co-transfection expression system as

335   described above for the SARS-CoV-2-pps, we produced pseudoviruses carrying the murine

15

336   leukemia virus (MLV) Env, MLV-pps, for use as a negative control (*41*). Percent neutralization

337   data were analyzed using GraphPad Prism 9.0.2 software. ID_{50}/IC_{50} values were calculated using

338   constraints for the percent neutralization (0-100%), whereas unconstrained neutralization plots

339   were shown in Fig 1 and fig S1.

340

341   **Histology, immunostaining, and imaging**

342   The mice were sacrificed 2 h to 8 weeks after a single-dose and 2 h to 5 weeks after the boost

343   immunization. The axillary, brachial, and popliteal sentinel lymph nodes were isolated for

344   histological analysis. Fresh lymph nodes were rapidly merged into frozen section compound

345   (VWR International, catalog no. 95057-838) in a plastic cryomold (Tissue-Tek at VWR, catalog

346   no. 4565) using liquid nitrogen to preserve the antigens on the cell membrane and spike. Lymph

347   node samples were stored at -80°C and sent to the Centre for Phenogenomics on dry ice for

348   further sample processing. Tissue sections (8 μm) were cut on a cryostat (Cryostar NX70) and

349   collected on charged slides. Sections were post-fixed in 10% neutral buffered formalin and

350   permeabilized in phosphate-buffered saline containing 0.5% Triton X-100 before

351   immunostaining. Protein Block (Agilent) was used to block nonspecific antibody binding before

352   incubating the sections with primary antibody overnight at 4°C. After washing in TBST, the

353   sections were incubated in fluorophore-conjugated secondary antibodies for 1 h at room

354   temperature. Lymph node tissue sections were stained with human anti-spike antibody P2B-2F6

355   (*45*) (1:50) and biotinylated goat anti-human secondary antibody (Abcam, catalog no. ab7152,

356   1:300), followed by streptavidin-horseradish peroxidase reagent (Vectastain Elite ABC-HRP Kit,

357   Vector, catalog no. PK-6100) then DAB (ImmPACT DAB, Vector, catalog no. SK-4105) to

358   study the distribution and retention of the S2GΔHR2 spike alone and S2GΔHR2-presenting E2p

16

359   and I3-01v9 SApNPs. For immunofluorescent staining, tissue sections were stained for FDCs

360   using anti-CD21 antibody (Abcam, catalog no. ab75985, 1:1800) followed by anti-rabbit

361   secondary antibody conjugated with Alexa Fluor 555 (Thermo Fisher, catalog no. A21428;

362   1:200), for B cells using anti-B220 antibody (eBioscience, catalog no. 14-0452-82, 1:100)

363   followed by anti-rat secondary antibody conjugated with Alexa Fluor 674 (Thermo Fisher,

364   catalog no. A21247; 1:200), and for subcapsular sinus macrophages using anti-sialoadhesin

365   (CD169) antibody (Abcam, catalog no. ab53443, 1:600) followed by anti-rat secondary antibody

366   conjugated with Alexa Fluor 488 (Abcam, catalog no. ab150165; 1:200). Germinal center B cells

367   were labeled using rat anti-GL7 antibody (FITC; BioLegend, catalog no. 144604, 1:250). T

368   Follicular helper cells were labeled using CD4 antibody (Biolegend, catalog no. 100402, 1:100)

369   followed by anti-rat secondary antibody conjugated with Alexa Fluor 488 (Abcam, catalog no.

370   ab150165; 1:1000) and Bcl6 antibody (Abcam, catalog no. ab220092, 1:300) followed by anti-

371   rabbit secondary antibody conjugated with Alexa Fluor 555 (Thermo Fisher, catalog no. A21428;

372   1:1000). Nuclei were then counterstained with DAPI (Sigma-Aldrich, catalog no. D9542, 100

373   ng/ml). The stained tissue sections were scanned using an Olympus VS-120 slide scanner and

374   imaged using a Hamamatsu ORCA-R2 C10600 digital camera for all bright-field and fluorescent

375   images. The bright-field images of stained S2GΔHR2 spike and S2GΔHR2-presenting SApNPs

376   in lymph node follicles and fluorescent images of GCs were quantified using ImageJ software

377   (National Institutes of Health) (*96*).

378

379   **Electron microscopy analysis of protein nanoparticles and lymph node tissues**

380   Electron microscopy (EM) analysis was performed by the Core Microscopy Facility at The

381   Scripps Research Institute. For negative-staining EM analysis of protein nanoparticles, the

17

382   S2GΔHR2-10GS-I3-01v9-L7P SApNP samples were prepared at the concentration of 0.01

383   mg/ml. Carbon-coated copper grids (400 mesh) were glow-discharged and 10 µL of each sample

384   was adsorbed for 2 min. Excess sample was wicked away and grids were negatively stained with

385   2% uranyl formate for 2 min. Excess stain was wicked away and the grids were allowed to dry.

386   For EM analysis of mouse tissues, the lymph nodes were dissected from each animal and

387   immersed in oxygenated 2.5% glutaraldehyde and 4% paraformaldehyde in 0.1M Na cacodylate

388   buffer (pH 7.4) fixative overnight at 4ºC (*97*). After washing in 0.1 M sodium cacodylate buffer,

389   the tissue samples were post-fixed in buffered 1% osmium tetroxide and 1.5% potassium

390   ferrocyanide for 1-1.5 h at 4°C, rinsed in the same buffer, and then stained *en bloc* with 0.5%

391   uranyl acetate overnight at 4°C. The tissue samples were washed in double-distilled H_2O and

392   dehydrated through a graded series of ethanol followed by acetone, infiltrated with LX-112

393   (Ladd) epoxy resin, and polymerized at 60°C. Ultrathin lymph node sections (at 70-nm

394   thickness) were prepared for imaging. Samples were analyzed at 80 kV with a Talos L120C

395   transmission electron microscope (Thermo Fisher) and images were acquired with a CETA 16M

396   CMOS camera.

397   **Lymph node disaggregation, cell staining, and flow cytometry**

398   Germinal center reactions, including the percentage of GC B cells (GL7$^+$B220$^+$) and T follicular

399   helper cells (CD3$^+$CD4$^+$CXCR5$^+$PD1$^+$), and the number of GC B cells and T follicular helper

400   cells were studied by flow cytometry (**fig. S5A**). The mice were sacrificed 2, 5, and 8 weeks after

401   a single-dose and 2 and 5 weeks after the boost immunization. Fresh axillary, brachial, and

402   popliteal sentinel lymph nodes were collected and mechanically disaggregated. These lymph

403   node samples were merged in enzyme digestion solution containing 958 µl of Hanks' balanced

404   salt solution (HBSS) buffer (Thermo Fisher Scientific, catalog no. 14185052), 40 µl of 10 mg/ml

18

405   collagenase IV (Sigma-Aldrich, catalog no. C5138), and 2 μl of 10 mg/ml of DNase (Roche,

406   catalog no. 10104159001) in an Eppendorf tube. After incubation at 37°C for 30 min, lymph

407   node samples were filtered through a 70 μm cell strainer and spun down at $400 \times g$ for 10 min.

408   The supernatant was discarded, and the cell pellet was resuspended in HBSS blocking solution

409   containing 0.5% (w/v) bovine serum albumin and 2 mM EDTA. The nonspecific binding of Fc

410   receptors was blocked using anti-CD16/32 antibody (BioLegend, catalog no. 101302) on ice for

411   30 min. Cocktail antibodies, Zombie NIR live/dead stain (BioLegend, catalog no. 423106),

412   Brilliant Violet 510 anti-mouse/human CD45R/B220 antibody (BioLegend, catalog no. 103247),

413   FITC anti-mouse CD3 antibody (BioLegend, catalog no. 100204), Alexa Fluor 700 anti-mouse

414   CD4 antibody (BioLegend, catalog no. 100536), PE anti-mouse/human GL7 antibody

415   (BioLegend, catalog no. 144608), Brilliant Violet 605 anti-mouse CD95 (Fas) antibody

416   (BioLegend, catalog no. 152612), Brilliant Violet 421 anti-mouse CD185 (CXCR5) antibody

417   (BioLegend, catalog no. 145511), and PE/Cyanine7 anti-mouse CD279 (PD-1) antibody

418   (BioLegend, catalog no. 135216) were then mixed with the cells and placed on ice for 30 min.

419   After washing the cell with HBSS blocking solution after antibody staining, the samples were

420   fixed using 1.6% paraformaldehyde (Thermo Fisher Scientific, catalog no. 28906) in HBSS on

421   ice for 30 min. The cell samples were stored in HBSS blocking solution for the flow cytometry

422   study. Sample events were acquired by a 5-laser BD Biosciences LSR II analytical flow

423   cytometer with BD FACS Diva 6 software at the Core Facility of The Scripps Research Institute.

424   The data were further processed using FlowJo 10 software.

425

426   **Statistical analysis**

427 Data were collected from 4-7 mice per group. All of the statistical analyses were performed and

428 graphs were generated using GraphPad Prism 6.01 software. For the antibody analysis,

429 comparisons between different vaccine groups were performed using two-tailed unpaired

430 Student's *t*-test. Comparisons of neutralizing antibody titers against SARS-CoV-2 variants were

431 performed using the same plasma samples and analyzed using two-tailed paired Student's *t*-test.

432 For the vaccine accumulation and GC study, comparisons between different vaccine groups were

433 performed using one-way analysis of variance (ANOVA) followed by Tukey's multiple

434 comparison *post hoc* test. Statistical significance was determined as ns: not significant, $*p <$

435 0.05, $**p < 0.01$, $***p < 0.001$, $****p < 0.0001$.

436

437 **SUPPLEMENTARY MATERIALS**

438 Supplementary material for this article is available at http://xxx/xxx/xxx.

439 **fig. S1**. Spike and spike-presenting SApNP vaccine-induced neutralizing antibody responses

440 against SARS-CoV-2 variants of concern (VOCs).

441 **fig. S2**. SARS-CoV-2 spike-presenting SApNP interaction with macrophages in a lymph node.

442 **fig. S3**. TEM images of SARS-CoV-2 spike-presenting I3-01v9 SApNP interaction with FDCs in

443 a lymph node.

444 **fig. S4**. Immunohistological analysis of SARS-CoV-2 spike/spike-presenting SApNP vaccine-

445 induced GCs.

446 **fig. S5**. Flow cytometry analysis of SARS-CoV-2 spike/spike-presenting SApNP vaccine-

447 induced GCs.

448 **fig. S6**. Adjuvant effect on SARS-CoV-2 spike/spike-presenting SApNP vaccine-induced GCs.

References

1. J. M. Dan *et al.*, Immunological memory to SARS-CoV-2 assessed for up to 8 months after infection. *Science* **371**, eabf4063 (2021).
2. B. Isho *et al.*, Persistence of serum and saliva antibody responses to SARS-CoV-2 spike antigens in COVID-19 patients. *Sci. Immunol.* **5**, eabe5511 (2020).
3. A. S. Iyer *et al.*, Persistence and decay of human antibody responses to the receptor binding domain of SARS-CoV-2 spike protein in COVID-19 patients. *Sci. Immunol.* **5**, eabe0367 (2020).
4. Y. Chen *et al.*, Quick COVID-19 healers sustain anti-SARS-CoV-2 antibody production. *Cell* **183**, 1496-1507.e1416 (2020).
5. S. Marot *et al.*, Rapid decline of neutralizing antibodies against SARS-CoV-2 among infected healthcare workers. *Nat. Commun.* **12**, 844 (2021).
6. R. Burioni, E. J. Topol, Assessing the human immune response to SARS-CoV-2 variants. *Nat. Med.*, Published Ahead-of-Print (2021).
7. H. Tegally *et al.*, Emergence of a SARS-CoV-2 variant of concern with mutations in spike glycoprotein. *Nature*, Published Ahead-of-Print (2021).
8. R. Challen *et al.*, Risk of mortality in patients infected with SARS-CoV-2 variant of concern 202012/1: matched cohort study. *BMJ* **372**, n579 (2021).
9. T. Kirby, New variant of SARS-CoV-2 in UK causes surge of COVID-19. *Lancet Respir. Med.* **9**, e20-e21 (2021).
10. N. G. Davies *et al.*, Estimated transmissibility and impact of SARS-CoV-2 lineage B.1.1.7 in England. *Science*, eabg3055 (2021).
11. N. L. Washington *et al.*, Genomic epidemiology identifies emergence and rapid transmission of SARS-CoV-2 B.1.1.7 in the United States. *medRxiv*, 2021.2002.2006.21251159 (2021).
12. E. C. Sabino *et al.*, Resurgence of COVID-19 in Manaus, Brazil, despite high seroprevalence. *Lancet* **397**, 452-455 (2021).
13. N. R. Faria *et al.*, Genomics and epidemiology of a novel SARS-CoV-2 lineage in Manaus, Brazil. *medRxiv*, 2021.2002.2026.21252554 (2021).
14. J. R. Mascola, B. S. Graham, A. S. Fauci, SARS-CoV-2 viral variants—tackling a moving target. *JAMA*, Published Ahead-of-Print (2021).
15. C. Zimmer, J. Corum, W. S.-L., in *Coronavirus vaccine tracker*. (https://www.nytimes.com/interactive/2020/science/coronavirus-vaccine-tracker.html).
16. N. Dagan *et al.*, BNT162b2 mRNA Covid-19 vaccine in a nationwide mass vaccination setting. *N. Engl. J. Med.*, Published Ahead-of-Print (2021).
17. L. R. Baden *et al.*, Efficacy and safety of the mRNA-1273 SARS-CoV-2 vaccine. *N. Engl. J. Med.* **384**, 403-416 (2020).
18. T. C. Williams, W. A. Burgers, SARS-CoV-2 evolution and vaccines: cause for concern? *Lancet Respir. Med.*, Published Ahead-of-Print (2021).
19. D. Y. Logunov *et al.*, Safety and efficacy of an rAd26 and rAd5 vector-based heterologous prime-boost COVID-19 vaccine: an interim analysis of a randomised controlled phase 3 trial in Russia. *Lancet* **397**, 671-681 (2021).
20. F. P. Polack *et al.*, Safety and efficacy of the BNT162b2 mRNA Covid-19 vaccine. *N. Engl. J. Med.* **383**, 2603-2615 (2020).

21. Q. Li *et al.*, The impact of mutations in SARS-CoV-2 spike on viral infectivity and antigenicity. *Cell* **182**, 1284-1294.e1289 (2020).

22. C. Rees-Spear *et al.*, The impact of spike mutations on SARS-CoV-2 neutralization. *bioRxiv*, 2021.2001.2015.426849 (2021).

23. C. K. Wibmer *et al.*, SARS-CoV-2 501Y.V2 escapes neutralization by South African COVID-19 donor plasma. *bioRxiv*, 2021.2001.2018.427166 (2021).

24. D. R. Burton, E. J. Topol, Variant-proof vaccines - invest now for the next pandemic. *Nature* **590**, 386-388 (2021).

25. M. Voysey *et al.*, Safety and efficacy of the ChAdOx1 nCoV-19 vaccine (AZD1222) against SARS-CoV-2: an interim analysis of four randomised controlled trials in Brazil, South Africa, and the UK. *Lancet* **397**, 99-111 (2021).

26. E. Andreano *et al.*, SARS-CoV-2 escape in vitro from a highly neutralizing COVID-19 convalescent plasma. *bioRxiv*, 2020.2012.2028.424451 (2020).

27. M. Hoffmann *et al.*, SARS-CoV-2 variants B.1.351 and P.1 escape from neutralizing antibodies. *Cell*, Published Ahead-of-Print (2021).

28. W. F. Garcia-Beltran *et al.*, Multiple SARS-CoV-2 variants escape neutralization by vaccine-induced humoral immunity. *Cell*, Published Ahead-of-Print (2021).

29. P. Wang *et al.*, Antibody resistance of SARS-CoV-2 variants B.1.351 and B.1.1.7. *bioRxiv*, 2021.2001.2025.428137 (2021).

30. P. Supasa *et al.*, Reduced neutralization of SARS-CoV-2 B.1.1.7 variant by convalescent and vaccine sera. *Cell*, Published Ahead-of-Print (2021).

31. D. A. Collier *et al.*, SARS-CoV-2 B.1.1.7 sensitivity to mRNA vaccine-elicited, convalescent and monoclonal antibodies. *medRxiv*, 2021.2001.2019.21249840 (2021).

32. Z. Wang *et al.*, mRNA vaccine-elicited antibodies to SARS-CoV-2 and circulating variants. *Nature*, Published Ahead-of-Print (2021).

33. Q. Li *et al.*, No higher infectivity but immune escape of SARS-CoV-2 501Y.V2 variants. *Cell*, Published Ahead-of-Print (2021).

34. A. Singh, Eliciting B cell immunity against infectious diseases using nanovaccines. *Nat. Nanotechnol.* **16**, 16-24 (2021).

35. G. D. Victora, M. C. Nussenzweig, Germinal centers. *Annu. Rev. Immunol.* **30**, 429-457 (2012).

36. R. Rappuoli, Glycoconjugate vaccines: principles and mechanisms. *Sci. Transl. Med.* **10**, eaat4615 (2018).

37. J. G. Cyster, C. D. C. Allen, B cell responses: cell Interaction dynamics and decisions. *Cell* **177**, 524-540 (2019).

38. M. McHeyzer-Williams, S. Okitsu, N. Wang, L. McHeyzer-Williams, Molecular programming of B cell memory. *Nat. Rev. Immunol.* **12**, 24-34 (2012).

39. M. Akkaya, K. Kwak, S. K. Pierce, B cell memory: building two walls of protection against pathogens. *Nat. Rev. Immunol.* **20**, 229-238 (2020).

40. N. S. De Silva, U. Klein, Dynamics of B cells in germinal centres. *Nat. Rev. Immunol.* **15**, 137-148 (2015).

41. L. He *et al.*, Single-component, self-assembling, protien nanoparticles presenting the receptor binding domain and stabilized spike as SARS-CoV-2 vaccine candidates. *Sci. Adv.* **7**, eabf1591 (2021).

42. K. H. D. Crawford *et al.*, Protocol and reagents for pseudotyping lentiviral particles with SARS-CoV-2 spike protein for neutralization assays. *Viruses* **12**, 513 (2020).

540 43. D. Wrapp *et al.*, Cryo-EM structure of the 2019-nCoV spike in the prefusion
541   conformation. *Science* **367**, 1260-1263 (2020).
542 44. D. Pinto *et al.*, Cross-neutralization of SARS-CoV-2 by a human monoclonal SARS-CoV
543   antibody. *Nature* **583**, 290-295 (2020).
544 45. B. Ju *et al.*, Human neutralizing antibodies elicited by SARS-CoV-2 infection. *Nature*
545   **584**, 115-119 (2020).
546 46. Y.-N. Zhang *et al.*, Nanoparticle size influences antigen retention and presentation in
547   lymph node follicles for humoral immunity. *Nano Lett.* **19**, 7226-7235 (2019).
548 47. B. A. Heesters, R. C. Myers, M. C. Carroll, Follicular dendritic cells: dynamic antigen
549   libraries. *Nat. Rev. Immunol.* **14**, 495-504 (2014).
550 48. J. G. Cyster, B cell follicles and antigen encounters of the third kind. *Nat. Immunol.* **11**,
551   989-996 (2010).
552 49. F. D. Batista, N. E. Harwood, The who, how and where of antigen presentation to B cells.
553   *Nat. Rev. Immunol.* **9**, 15-27 (2009).
554 50. M. Kuka, M. Iannacone, Viral subversion of B cell responses within secondary lymphoid
555   organs. *Nat. Rev. Immunol.* **18**, 255-265 (2018).
556 51. R. Rappuoli, D. Serruto, Self-assembling nanoparticles usher in a new era of vaccine
557   design. *Cell* **176**, 1245-1247 (2019).
558 52. C. D. C. Allen, T. Okada, J. G. Cyster, Germinal-center organization and cellular
559   dynamics. *Immunity* **27**, 190-202 (2007).
560 53. C. D. C. Allen, J. G. Cyster, Follicular dendritic cell networks of primary follicles and
561   germinal centers: Phenotype and function. *Semin. Immunol.* **20**, 14-25 (2008).
562 54. L. Mesin, J. Ersching, Gabriel D. Victora, Germinal center B cell dynamics. *Immunity* **45**,
563   471-482 (2016).
564 55. N. Baumgarth, The shaping of a B cell pool maximally responsive to infections. *Annu.*
565   *Rev. Immunol.* **39**, (2021).
566 56. J. López-Sagaseta, E. Malito, R. Rappuoli, M. J. Bottomley, Self-assembling protein
567   nanoparticles in the design of vaccines. *Comput. Struct. Biotechnol. J.* **14**, 58-68 (2016).
568 57. D. J. Irvine, M. C. Hanson, K. Rakhra, T. Tokatlian, Synthetic nanoparticles for vaccines
569   and immunotherapy. *Chem. Rev.* **115**, 11109-11146 (2015).
570 58. D. J. Irvine, M. A. Swartz, G. L. Szeto, Engineering synthetic vaccines using cues from
571   natural immunity. *Nat. Mater.* **12**, 978-990 (2013).
572 59. S. Crotty, Follicular helper CD4 T cells (TFH). *Annu. Rev. Immunol.* **29**, 621-663 (2011).
573 60. A K Szakal, a. M H Kosco, J. G. Tew, Microanatomy of lymphoid tissue during humoral
574   immune responses: structure function relationships. *Annu. Rev. Immunol.* **7**, 91-109
575   (1989).
576 61. J. Merkenschlager *et al.*, Dynamic regulation of TFH selection during the germinal centre
577   reaction. *Nature* **591**, 458-463 (2021).
578 62. Z. Shulman *et al.*, T follicular helper cell dynamics in germinal centers. *Science* **341**,
579   673-677 (2013).
580 63. K. Lederer *et al.*, SARS-CoV-2 mRNA vaccines foster potent antigen-specific germinal
581   center responses associated with neutralizing antibody generation. *Immunity* **53**, 1281-
582   1295.e1285 (2020).
583 64. T. Tokatlian *et al.*, Innate immune recognition of glycans targets HIV nanoparticle
584   immunogens to germinal centers. *Science* **363**, 649-654 (2019).

585 65. S. N. Mueller, S. Tian, J. M. DeSimone, Rapid and persistent delivery of antigen by
586   lymph node targeting PRINT nanoparticle vaccine carrier to promote humoral immunity.
587   *Mol. Pharm.* **12**, 1356-1365 (2015).

588 66. B. Zhang *et al.*, A platform incorporating trimeric antigens into self-assembling
589   nanoparticles reveals SARS-CoV-2-spike nanoparticles to elicit substantially higher
590   neutralizing responses than spike alone. *Sci. Rep.* **10**, 18149 (2020).

591 67. A. C. Walls *et al.*, Elicitation of potent neutralizing antibody responses by designed
592   protein nanoparticle vaccines for SARS-CoV-2. *Cell* **183**, 1367-1382.e1317 (2020).

593 68. A. E. Powell *et al.*, A single immunization with spike-functionalized ferritin vaccines
594   elicits neutralizing antibody responses against SARS-CoV-2 in mice. *ACS Cent. Sci.* **7**,
595   183-199 (2021).

596 69. P. J. M. Brouwer *et al.*, Two-component spike nanoparticle vaccine protects macaques
597   from SARS-CoV-2 infection. *Cell* **184**, 1188-1200.e1119 (2021).

598 70. K. S. Park *et al.*, Lipid-based vaccine nanoparticles for induction of humoral immune
599   responses against HIV-1 and SARS-CoV-2. *J. Control. Release* **330**, 529-539 (2021).

600 71. Y.-F. Kang *et al.*, Rapid development of SARS-CoV-2 spike protein receptor-binding
601   domain self-assembled nanoparticle vaccine candidates. *ACS Nano* **15**, 2738-2752
602   (2021).

603 72. J. H. Lam *et al.*, Next generation vaccine platform: polymersomes as stable nanocarriers
604   for a highly immunogenic and durable SARS-CoV-2 spike protein subunit vaccine.
605   *bioRxiv*, 2021.2001.2024.427729 (2021).

606 73. A. A. Cohen *et al.*, Mosaic nanoparticles elicit cross-reactive immune responses to
607   zoonotic coronaviruses in mice. *Science* **371**, 735-741 (2021).

608 74. W. C. Huang *et al.*, SARS-CoV-2 RBD neutralizing antibody induction is enhanced by
609   particulate vaccination. *Adv. Mater.* **32**, e2005637 (2020).

610 75. T. K. Tan *et al.*, A COVID-19 vaccine candidate using SpyCatcher multimerization of
611   the SARS-CoV-2 spike protein receptor-binding domain induces potent neutralising
612   antibody responses. *Nat. Commun.* **12**, 542 (2021).

613 76. D. Lainšček *et al.*, Immune response to vaccine candidates based on different types of
614   nanoscaffolded RBD domain of the SARS-CoV-2 spike protein. *bioRxiv*,
615   2020.2008.2028.244269 (2020).

616 77. X. Ma *et al.*, Nanoparticle vaccines based on the receptor binding domain (RBD) and
617   heptad repeat (HR) of SARS-CoV-2 elicit robust protective immune responses. *Immunity*
618   **53**, 1315-1330.e1319 (2020).

619 78. N. C. Dalvie *et al.*, Engineered SARS-CoV-2 receptor binding domain improves
620   immunogenicity in mice and elicits protective immunity in hamsters. *bioRxiv*,
621   2021.2003.2003.433558 (2021).

622 79. R. Rappuoli *et al.*, Vaccinology in the post–COVID-19 era. *Proc. Natl. Acad. Sci. U.S.A.*
623   **118**, e2020368118 (2021).

624 80. M. Jeyanathan *et al.*, Immunological considerations for COVID-19 vaccine strategies.
625   *Nat. Rev. Immunol.* **20**, 615-632 (2020).

626 81. L. Corey, J. R. Mascola, A. S. Fauci, F. S. Collins, A strategic approach to COVID-19
627   vaccine R&D. *Science* **368**, 948-950 (2020).

628 82. L. DeFrancesco, Whither COVID-19 vaccines? *Nat. Biotechnol.* **38**, 1132-1145 (2020).

629 83.   P. S. Arunachalam *et al.*, Adjuvanting a subunit SARS-CoV-2 nanoparticle vaccine to
630   induce protective immunity in non-human primates. *bioRxiv*, 2021.2002.2010.430696
631   (2021).
632 84.   P. J. Hotez, D. B. Corry, U. Strych, M. E. Bottazzi, COVID-19 vaccines: neutralizing
633   antibodies and the alum advantage. *Nat. Rev. Immunol.* **20**, 399-400 (2020).
634 85.   S. P. Kasturi *et al.*, Programming the magnitude and persistence of antibody responses
635   with innate immunity. *Nature* **470**, 543-547 (2011).
636 86.   S. G. Reed, M. T. Orr, C. B. Fox, Key roles of adjuvants in modern vaccines. *Nat. Med.*
637   **19**, 1597-1608 (2013).
638 87.   T.-Y. Kuo *et al.*, Development of CpG-adjuvanted stable prefusion SARS-CoV-2 spike
639   antigen as a subunit vaccine against COVID-19. *Sci. Rep.* **10**, 20085 (2020).
640 88.   J.-H. Tian *et al.*, SARS-CoV-2 spike glycoprotein vaccine candidate NVX-CoV2373
641   immunogenicity in baboons and protection in mice. *Nat. Commun.* **12**, 372 (2021).
642 89.   C. Keech *et al.*, Phase 1–2 trial of a SARS-CoV-2 recombinant spike protein nanoparticle
643   vaccine. *N. Engl. J. Med.* **383**, 2320-2332 (2020).
644 90.   I. Quast, D. Tarlinton, B cell memory: understanding COVID-19. *Immunity* **54**, 205-210
645   (2021).
646 91.   D. J. Irvine, B. J. Read, Shaping humoral immunity to vaccines through antigen-
647   displaying nanoparticles. *Curr. Opin. Immunol.* **65**, 1-6 (2020).
648 92.   M. D. Shin *et al.*, COVID-19 vaccine development and a potential nanomaterial path
649   forward. *Nat. Nanotechnol.* **15**, 646-655 (2020).
650 93.   L. He *et al.*, Proof of concept for rational design of hepatitis C virus E2 core nanoparticle
651   vaccines. *Sci. Adv.* **6**, eaaz6225 (2020).
652 94.   L. He *et al.*, Single-component multilayered self-assembling nanoparticles presenting
653   rationally designed glycoprotein trimers as Ebola virus vaccines. *bioRxiv*,
654   2020.2008.2022.262634 (2020).
655 95.   L. He *et al.*, HIV-1 vaccine design through minimizing envelope metastability. *Sci. Adv.*
656   **4**, aau6769 (2018).
657 96.   C. A. Schneider, W. S. Rasband, K. W. Eliceiri, NIH Image to ImageJ: 25 years of image
658   analysis. *Nat. Methods* **9**, 671-675 (2012).
659 97.   T. J. Johnson, Glutaraldehyde fixation chemistry: oxygen-consuming reactions. *Eur. J.*
660   *Cell Biol.* **45**, 160-169 (1987).
661

662 **Acknowledgements**

681

682   **Figure Legends**

683   **Fig. 1. SARS-CoV-2 SApNP vaccines induce broadly neutralizing antibody responses to**

684   **three variants of concern.** (**A**) Molecular surface representations of vaccine constructs,

685   including two spikes (S2P$_{ECTO}$-5GS-1TD0 and S2GΔHR2-5GS-1TD0) and three spike-

686   presenting SApNPs (S2GΔHR2-5GS-ferritin (FR), S2GΔHR2-5GS-E2p-LD4-PADRE (E2p-

687   L4P), and S2GΔHR2-10GS-I3-01v9-LD7-PADRE (I3-01v9-L7P)). Representative negative-

688   stain EM (nsEM) image of S2GΔHR2-10GS- I3-01v9-L7P SApNPs is shown on the right. (**B**)

689   Neutralization of the original Wuhan-Hu-1 strain by mouse plasma induced by 5 different

690   vaccines at week 5 after two intraperitoneal injections. ID$_{50}$ titers derived from SARS-CoV-2-pp

691   neutralization assays are plotted, with average ID$_{50}$ values labeled on the plots. (**C**) Mouse

692   plasma neutralization against the original Wuhan-Hu-1 strain and three variants, B.1.1.7, B1.351,

693   and P.1, at week 5 after two intraperitoneal injections of the adjuvanted S2GΔHR2-10GS-I3-

694   01v9-L7P vaccine. Left panels 1-4: percent neutralization plots of individual mice against 4

695   SARS-CoV-2 strains; Right panel: ID$_{50}$ plot. In (B) and (C), the plasma samples were generated

696   in the previous study (*41*), where mice were immunized with 50 μg of adjuvanted vaccine

697   antigen. (**D**) Neutralization of the original Wuhan-Hu-1 strain by mouse plasma induced the

698   S2GΔHR2 spike and two large S2GΔHR2-presenting SApNPs. Vaccines were administered via

699   footpad injections (0.8 μg/injection, for a total of 3.3 μg/mouse). (**E**) Mouse plasma

700   neutralization against the original Wuhan-Hu-1 strain and three variants, B.1.1.7, B1.351, and

701   P.1, at week 5 after two footpad injections of the S2GΔHR2 spike and two large S2GΔHR2-

702   presenting SApNPs. In (B)-(E), the ID$_{50}$ values are plotted as mean ± SEM. The data were

703   analyzed using two-tailed unpaired Student's *t*-test for comparison between different vaccine

704   groups or two-tailed paired Student's *t*-test for comparison of ID$_{50}$ titers against SARS-Cov-2

27

705   variants using the same plasma samples from a mouse. *$p < 0.05$, **$p < 0.01$. (**F**) Neutralization

706   of four SARS-CoV-2 strains by human monoclonal antibodies including CR3022, B38, CB6,

707   S309, CC12.1, CC12.3, C105, and P2B-2F6. IC_{50} values are listed and color-coded (white: no

708   neutralization; green to red: low to high). The IC_{50} values were calculated with the

709   %neutralization range constrained within 0.0-100.0%.

710

711   **Fig. 2. SARS-CoV-2 SApNP vaccines induce long-term lymph node follicle retention.** (**A**, **B**)

712   S2GΔHR2-presenting I3-01v9 SApNP vaccine distribution in a lymph node 12 h after (**A**) a

713   single-dose or (**B**) prime-boost footpad injections (10 μg/injection, 40 μg/mouse). Schematic

714   illustration of SApNPs in lymph node follicles is shown. (**C**, **D**) Histological images of the

715   S2GΔHR2 spike and S2GΔHR2-presenting E2p and I3-01 SApNP vaccine trafficking and

716   retention in lymph node follicles 2 h to 8 weeks after (**C**) a single-dose or (**D**) prime-boost

717   injections. (**E**, **F**) Quantification of vaccine accumulation in lymph node follicles 48 h after (**E**) a

718   single-dose or (**F**) prime-boost injections. Data were collected from more than 10 lymph node

719   follicles (*n* = 3-4 mice/group). The data points are expressed as mean ± SD. The data were

720   analyzed using one-way ANOVA followed by Tukey's multiple comparison *post hoc* test. **$p <$

721   0.01, ***$p < 0.001$, ****$p < 0.0001$.

722

723   **Fig. 3. SARS-CoV-2 SApNP vaccines interact with follicular dendritic cells (FDCs) and are**
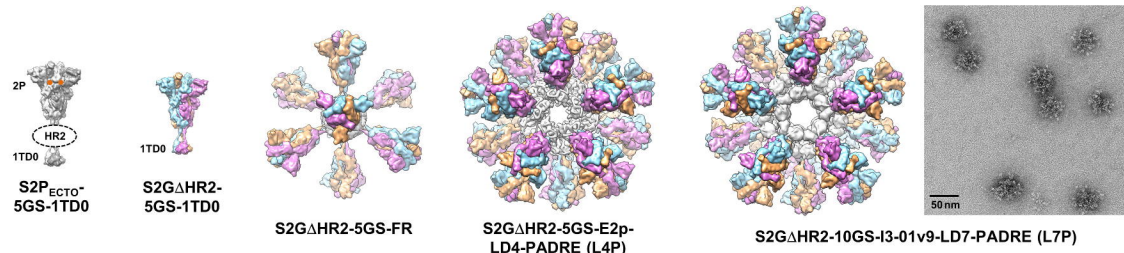
724   **presented on FDC dendrites to B cells.** (**A**, **B**) S2GΔHR2 spike and S2GΔHR2-presenting E2p

725   and I3-01 SApNP vaccine interaction with FDC networks in lymph node follicles 12 h after (**A**)

726   a single-dose or (**B**) prime-boost injections (10 μg/injection, 40 μg/mouse). Vaccine antigens (the

727   S2GΔHR2 spike and S2GΔHR2-presenting E2p and I3-01 SApNPs) colocalized with FDC

728 networks. Immunostaining is color-coded (Green: CD21; Red: CD169; White: anti-spike). (**C**)

729 Representative TEM images of an FDC surrounded by multiple B cells. S2GΔHR2-presenting

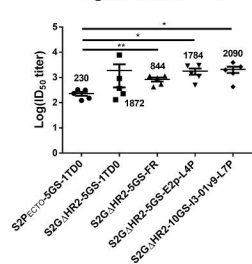730 I3-01 SApNPs (yellow arrows) presented on FDC dendrites.

731

732 **Fig. 4. SARS-CoV-2 SApNP vaccines induce robust long-lived germinal centers.** (**A**) Top:

733 Representative immunohistological images of germinal centers at week 2 after a single-dose

734 injection of the S2GΔHR2-presenting I3-01 SApNP vaccine (10 μg/injection, 40 μg/mouse).

735 Bottom: germinal center B cells (GL7$^+$, red) adjacent to FDCs (CD21$^+$, green) in lymph node

736 follicles (left), and T_{fh} cells in the light zone (LZ) of germinal centers (right). (**B**, **C**)

737 Quantification of germinal center reactions using immunofluorescent images: GC/FDC ratio and

738 sizes of germinal centers 2, 5, and 8 weeks after (**B**) a single-dose or (**C**) prime-boost injections

739 (n = 4-7 mice/group). The GC/FDC ratio is defined as whether germinal center formation is

740 associated with an FDC network (%). Representative immunohistological images of germinal

741 centers in mice immunized using S2GΔHR2 spike or S2GΔHR2-presenting E2p and I3-01

742 SApNP vaccines at week 8 after (**D**) a single-dose or (**E**) prime-boost injections. (**F**, **G**)

743 Quantification of germinal center reactions using flow cytometry: percentage and number of

744 germinal center B cells and T follicular helper cells 2, 5, and 8 weeks after (**F**) a single-dose or

745 (**G**) prime-boost injections. The data points are shown as mean ± SD. The data were analyzed

746 using one-way ANOVA followed by Tukey's multiple comparison *post hoc* test for each

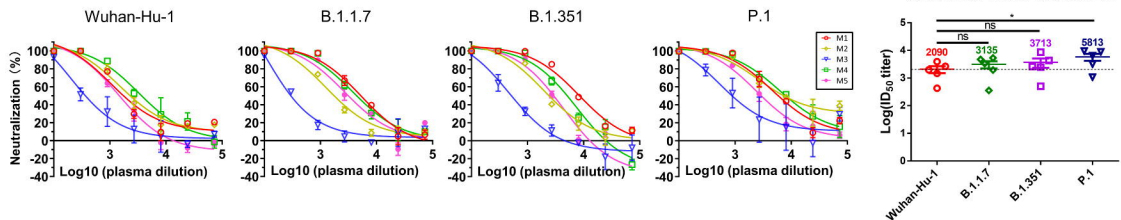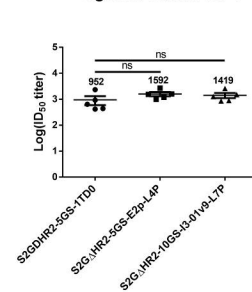747 timepoint. *$p < 0.05$, **$p < 0.01$, ***$p < 0.001$, ****$p < 0.0001$.

Figure 1

A

S2P$_{ECTO}$-5GS-1TD0

S2GΔHR2-5GS-1TD0

S2GΔHR2-5GS-FR

S2GΔHR2-5GS-E2p-LD4-PADRE (L4P)

S2GΔHR2-10GS-I3-01v9-LD7-PADRE (L7P)

50 nm

B Mouse plasma neutralization against Wuhan-Hu-1

C Mouse plasma neutralization against SARS-CoV-2 variants

Wuhan-Hu-1

B.1.1.7

B.1.351

P.1

S2GΔHR2-10GS-I3-01v9-L7P

D Mouse plasma neutralization against Wuhan-Hu-1

E Mouse plasma neutralization against SARS-CoV-2 variants

S2GΔHR2-5GS-1TD0

S2GΔHR2-5GS-E2p-L4P

S2GΔHR2-10GS-I3-01v9-L7P
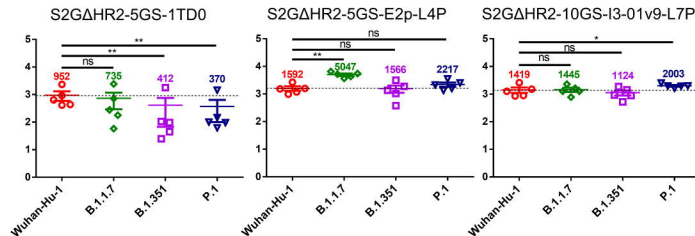
F Human monoclonal antibody neutralization against SARS-CoV-2 variants

mAb	Wuhan-Hu-1	B.1.1.7	B.1.351	P.1
CR3022	>10 µg/ml	>10 µg/ml	>10 µg/ml	>10 µg/ml
B38	0.700	>10 µg/ml	>10 µg/ml	>10 µg/ml
CB6	0.036	0.160	>10 µg/ml	>10 µg/ml
S309	8.222	3.217	0.148	0.107
CC12.1	0.049	0.205	>10 µg/ml	8.326
CC12.3	0.034	0.064	>10 µg/ml	>10 µg/ml
C105	0.412	0.452	>10 µg/ml	>10 µg/ml
P2B-2F6	0.837	0.352	>10 µg/ml	>10 µg/ml

Figure 2

Figure 3

A Single-dose - 12h

S2GΔHR2 spike | E2p SApNP | I3-01v9 SApNP | CD169/CD21 | Spike (anti-spike Abs)

B Prime-boost - 3w + 12h

S2GΔHR2 spike | E2p SApNP | I3-01v9 SApNP | CD169/CD21 | Spike (anti-spike Abs)
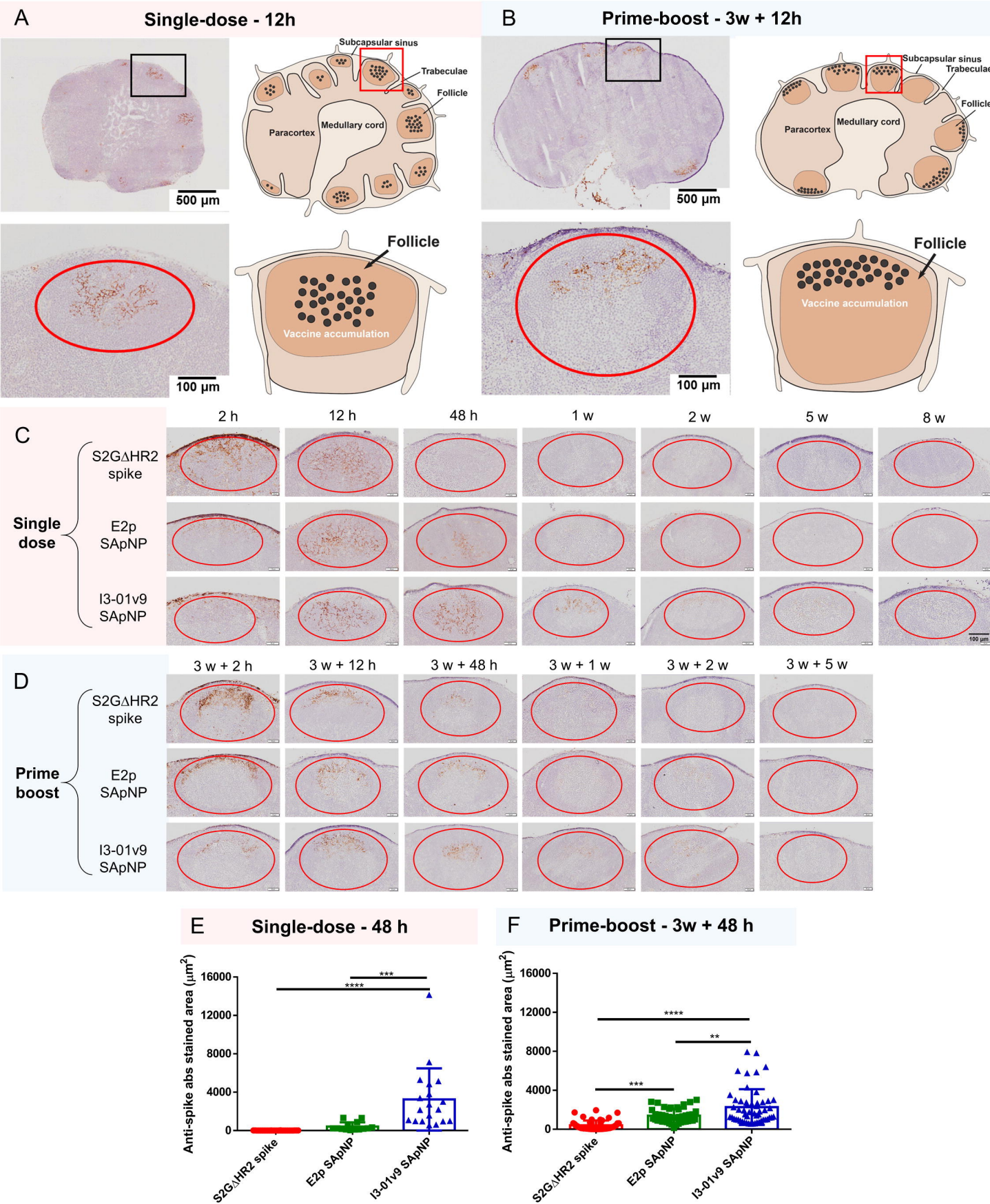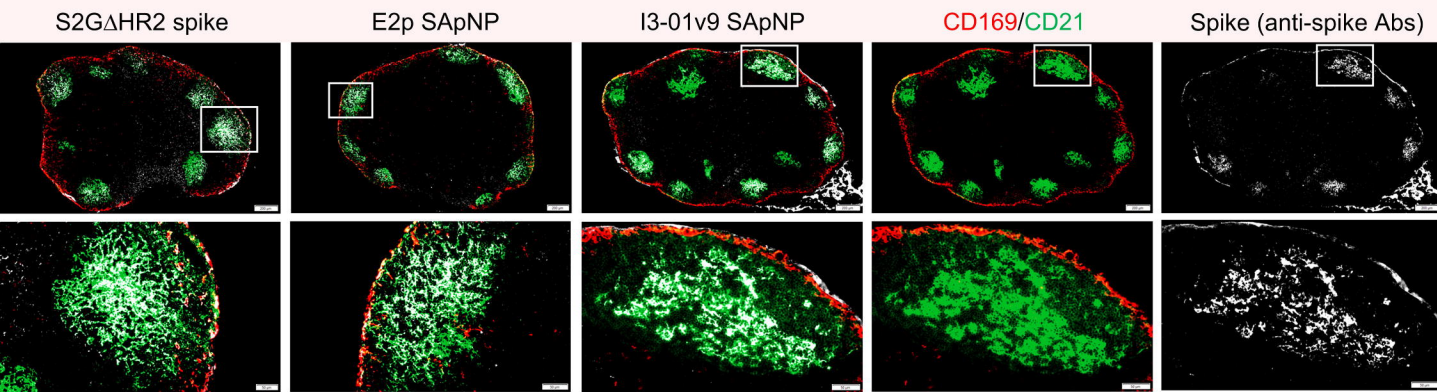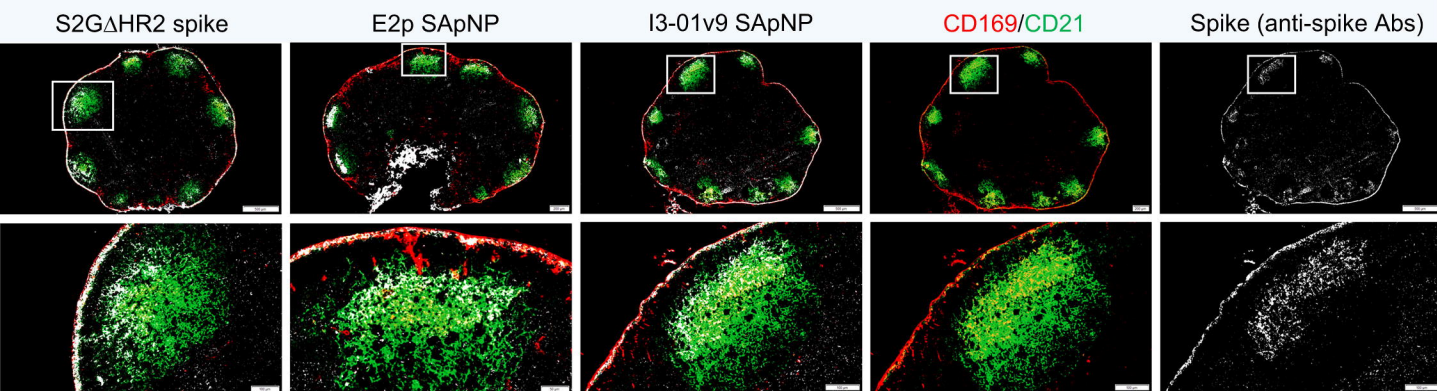
C I3-01v9 SApNPs (yellow arrow) are aligned on FDC dendrites

Figure 4

A — Germinal center (GC) B cells — GL7/CD21/B220 — LZ, FDCs, DZ, GC B cells — T follicular helper (T$_{fh}$) cells — CD4/Bcl6/DAPI — T$_{fh}$ cells

B — **Single-dose** — GC/FDC ratio (%); GC area (μm²); Weeks 2, 5, 8 — S2GΔHR2 spike, E2p SApNP, I3-01v9 SApNP

C — **Prime-boost** — GC/FDC ratio (%); GC area (μm²); Weeks 5, 8

D — **Single-dose - 8 w** — GL7/CD21/B220; CD4/Bcl6/DAPI — S2GΔHR2 spike, E2p SApNP, I3-01v9 SApNP

E — **Prime-boost - 3 w + 5 w** — GL7/CD21/B220; CD4/Bcl6/DAPI

F — **Single-dose** — GC B cells; T$_{fh}$ cells; % of GC B cells; % of T$_{fh}$ cells; No. of GC B cells; No. of T$_{fh}$ cells; weeks 2, 5, 8

G — **Prime-boost** — GC B cells; T$_{fh}$ cells; % of GC B cells; % of T$_{fh}$ cells; No. of GC B cells; No. of T$_{fh}$ cells; weeks 5, 8